A two-phase model for the development of positive surface discharge in air

Tran Nam Trung
Vietnam Electricity
Igor O Golosnoy, Paul L Lewin
School of Electronics and Computer Science, University of Southampton
Tran Khanh Viet Dung
Vietnam Oil and Gas Group

Abstract

This paper is concerned with the simulation of positive surface discharge - a frequently encountered phenomenon in high voltage electrical equipment. The development of a filamentary positive surface discharge in air is simulated using the hydrodynamic drift-diffusion approximation. The model consists of a set of continuity equations accounting for the movement, generation and loss of charge carriers (electrons, positive and negative ions). The continuity equations are coupled with Poisson's equation to take into account the effect of space charge on the electric field. The discharge is separated into two phases: the axial propagation of a streamer in the gas gap between a needle electrode and an insulator in phase I and the radial development of the streamer along the dielectric surface in phase II. The first phase is simulated in 2D axial symmetry using the finite element method. In phase II, the streamer is assumed to occupy a cylindrical channel of fixed radius and is solved in 1D using the accurate finite-volume flux-corrected transport algorithm. It is found that the streamer dynamics are strongly governed by the electric field created by the dielectric barrier. Comparisons between simulation results and experimental measurements are also made.

1. Introduction

The generation of non-thermal plasmas has been a topic of interest in recent years due to the broad range of applications it may offer. Most applications utilise the dielectric barrier discharge (DBD) arrangement to effectively control the current and charge distribution [1, 2]. At atmospheric pressure, DBDs have found their applications in large-scale ozone production, plasma display panels, thin film deposition, actuators for flow control, CO_2 lasers and excimer ultra-violet light sources [1, 3]. Surface discharges at triple-junctions in gas-insulated switchgear (GIS) have also attracted a large amount of research due to their critical influence on insulation system coordination.

It has been well established that the discharge pattern depends on the applied voltage polarity. A negative discharge produces a diffuse/circular form of surface charge [4, 5] whilst a positive discharge generates a filamentary streamer structure [6 - 8]. The surface charge distribution can be measured using dust Figures, Lichtenberg Figures, electrostatic probes or the Pockels technique [9, 10]. Out of these methods, the Pockels technique is the only method that provides quantitative analysis of the discharge dynamics.

The simulation of surface discharge phenomena provides better understanding of charge accumulation processes, facilitates effective control over the discharge parameters and is a useful tool for insulation system dimensioning. The modelling of a negative surface discharge has been reported in 2D axial symmetry space dimension [11]. In this paper, the development of a positive surface streamer is simulated and compared with experimental Pockels results. The hydrodynamic drift-diffusion approach is utilised which consists of coupled continuity equations for the charge transport and Poisson's equation for the electric field distribution [1]. The simulation consists of two phases: the axial propagation of streamer in the gas gap between a needle electrode and an insulator and the radial development along the dielectric surface. The second phase of the model helps

to capture the streamer dynamics under different electric fields using reasonable simplifications.

2. Experiment

Fig. 1 shows the schematic diagram of the Pockels experiment to measure surface discharge dynamics. A 17mW HeNe laser source is utilised to generate a coherent polarised light of 632.8nm wavelength. The light is expanded to a diameter of 30mm using a Galilean beam expander prior to arriving at the polarising beam splitter (PBS). The PBS serves as both a polariser and analyser. Having passed through the PBS, the input light is horizontally polarised. It is then modulated by an optical phase modulator (OPM), which is stressed with a square pulse waveform generated from an amplifier. The OPM is made of a 1mm thick Bismuth Silicon Oxide (BSO) crystal with the principal axes positioned 45° with respect to the horizontal. The sensing Pockels crystal is wedge polished to approximate dimensions of 20 × 20 × 0.16mm^3 and glued to a 0.8mm thick BK7 glass with one side grounded via a transparent electrode (Indium Tin Oxide). A needle electrode of 25μm radius of curvature is placed 500μm distant away from the other side of the crystal in order to avoid any undesired mechanical birefringence. The applied voltage waveform is programmed by a function generator and amplified using a high voltage amplifier. The discharge crystal is housed in a vacuum chamber connected to a vacuum pump or an air compressor and a pressure gauge. Light reflected from the back-face of the crystal passes through the PBS again and only the vertical component of the light is transmitted to the CCD camera. The lens and pinhole are placed in between the PBS and camera in order to block unnecessary reflections. The OPM operation, discharge triggering process and camera capturing are all synchronised by the synchronisation control circuit (SCC) programmed in a peripheral interface controller (PIC). Images obtained from the camera are transferred to a personal computer for further image processing after each experiment.

The principle of the electro-optic experiment is based on the Pockels characteristic of some materials such as BSO. Under the electric field induced by surface charge, the refractive indexes of the BSO crystal along two perpendicular principal axes (so-called fast and slow axes) are altered. The change in the refractive indexes leads to a linear phase retardation of the incident light. The change in phase is linearly proportional to the internal electric field. By measuring intensity of the reflected light, the phase retardation can be determined and hence the surface charge density. Further details of the experiment can be found in Y L Sam et al [9]. Similar experimental arrangement and results have also been reported in D Tanaka et al [6].

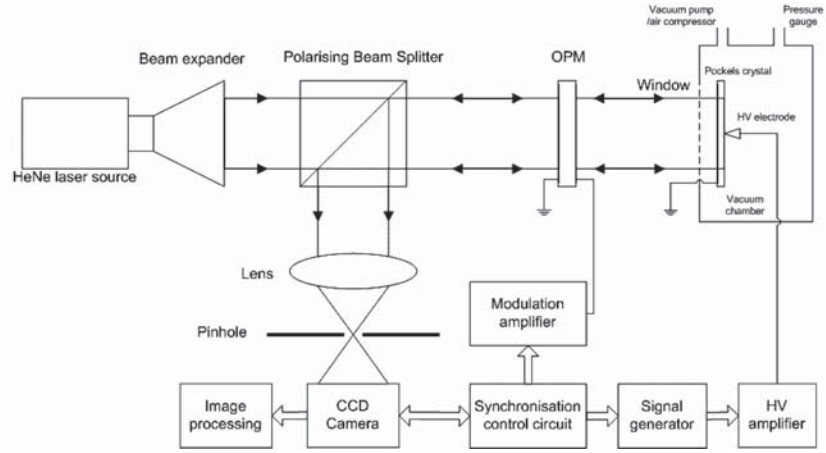

Fig. 1. *Schematic diagram of the Pockels experiment*

3. Model description

3.1. Governing equations

Based on the well-known hydrodynamic drift-diffusion model [1, 12], the set of continuity equations (to account for the movement, generation and loss of electrons, positive and negative ions and for the development of space charge) coupled with Poisson's equation (to include the effect of space charge on the electric field) is given as:

$$\frac{\partial N_e}{\partial t} = S + N_e\alpha\left|\overrightarrow{W_e}\right| - N_e\eta\left|\overrightarrow{W_e}\right| - N_eN_p\beta_{ep} - \nabla.\left(N_e\overrightarrow{W_e} - D_e\nabla N_e\right) \quad (1)$$

$$\frac{\partial N_p}{\partial t} = S + N_e\alpha\left|\overrightarrow{W_e}\right| - N_nN_p\beta_{np} - N_eN_p\beta_{ep} - \nabla.\left(N_p\overrightarrow{W_p} - D_p\nabla N_p\right) \quad (2)$$

$$\frac{\partial N_n}{\partial t} = N_e\eta\left|\overrightarrow{W_e}\right| - N_nN_p\beta_{np} - \nabla.\left(N_n\overrightarrow{W_n} - D_n\nabla N_n\right) \quad (3)$$

$$\nabla.\left(\varepsilon_r\nabla V\right) + \frac{e}{\varepsilon_0}\left(N_p - N_e - N_n\right) = 0 \quad (4)$$

Where t is time, e the electronic charge, ε_0 the vacuum permittivity and ε_r the relative permittivity of the medium, V the electric potential; N_e, N_p and N_n the electron, positive and negative ion concentrations respectively; $\overrightarrow{W_e}$, $\overrightarrow{W_p}$ and $\overrightarrow{W_n}$ the electron, positive and negative ion drift velocities; α, η, β, D_e, D_p and D_n the ionisation, attachment, recombination and diffusion coefficients for electrons and positive and negative ions respectively. The source term S represents the photoionisation process. The swarm parameters, which are functions of the local electric field, $\vec{E} = -\nabla V$, are extracted from the approximations published in [13] and modifications detailed in [14].

3.2. Computational domain

The simulation geometry utilised in this work is shown in Fig. 2. A hyperboloid needle electrode of 25µm radius of curvature was modelled. A system of two dielectric layers was utilised to resemble the Pockels cell. A 160µm thick BSO layer (ε_r = 56) was set on top of an 800 µm thick glass (ε_r = 3). Both layers share the same radius of 10mm. The BSO surface was set 500µm away from the needle electrode. The ground electrode was set at the bottom of the glass. The simulation domain dimensions are 10mm by 10mm. Unless otherwise stated the model assumes atmospheric pressure and room temperature.

3.3. Numerical algorithm and boundary conditions

Equations 1 - 4 should ideally be solved in 3D due to the asymmetry of the streamer pattern. However, this approach was found ineffective as it would have cost a vast amount of computational time and resources. In this paper, the simulation of a positive surface discharge is separated into two phases. In the first phase, due to the strong axial electric field at the needle tip a streamer forms and travels towards the insulator. This phase was fully simulated in 2D axial symmetry space dimension (effectively 3D). When the streamer arrives at the dielectric surface, the dielectric acts as an impermeable barrier causing the discharge to develop along the surface. All barrier discharge models to date continue simulating the discharge in the same 2D space dimension [15 - 17]. This results in a ring form of the streamer. Nonetheless from experimental results, the streamer does not expand radially but rather forms filamentary branches. The branching phenomena have been attributed to instabilities and asymmetric distribution of electrons where the gas streamer interacts with the dielectric surface [18]. For this reason, the second phase of the model proposed in this paper describes the development of one particular streamer along the surface. This phase was simulated in 1D by assuming the streamer propagates along the insulator surface in the form of a cylindrical channel of fixed radius. The radial field calculated at the end of the first phase is used as the driving force for the streamer development in the second phase.

The first phase was solved using the conventional finite element method with an addition of streamline artificial anisotropic diffusion [9]. This approach has proved effective in solving discharge problems in gas and liquid [20, 21] although other advanced techniques for transport problems can be used [22].

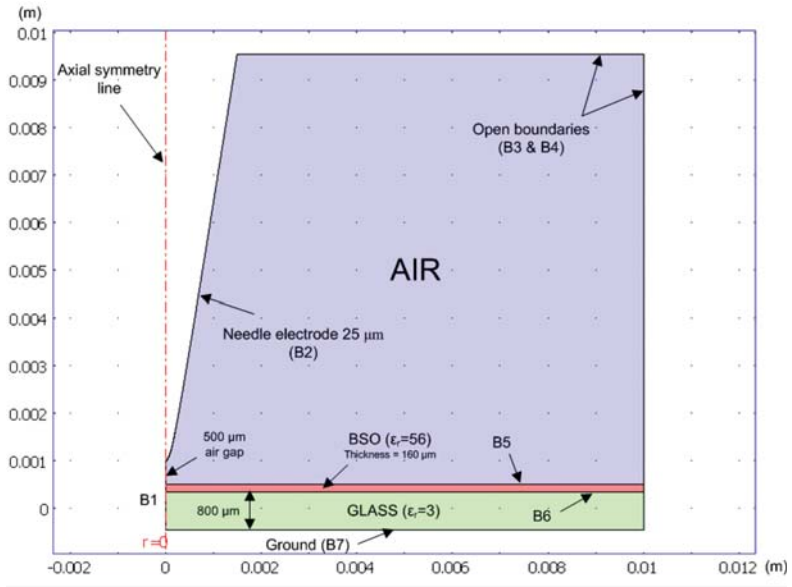

Fig. 2. *Positive surface discharge model geometry*

With regard to the meshing of the geometry, a mesh size of 2.5µm in the region near the symmetry axis and the needle electrode was found sufficient to simulate the development of a streamer in phase I. The total number of mesh elements created was approximately 150,000 giving rise to just above 1 million degrees of freedom to solve. In the first phase, the time steps vary in the range of 10^{-13} - 10^{-11}s. The total runtime was under 6 hours using a single core 3 GB RAM personal computer.

Boundary conditions for the first phase are summarised in Table 1. The boundary conditions of interest are those at the gas-insulator interface (B5). There are generally two types of boundary condition for this

Table 1. *Boundary conditions for the second phase of the positive surface discharge model with reference to Fig. 2*

	Boundary conditions for N_e	Boundary conditions for N_p	Boundary conditions for N_n	Boundary conditions for V
Boundary 1	$\frac{\partial N_e}{\partial r}=0$	$\frac{\partial N_p}{\partial r}=0$	$\frac{\partial N_n}{\partial r}=0$	$\frac{\partial V}{\partial r}=0$
Boundary 2	$\vec{n}\cdot(-D_e\nabla N_e)=0$	$\vec{n}\cdot(\overrightarrow{W_p}N_p - D_p\nabla N_p)=0$	$\vec{n}\cdot(-D_n\nabla N_n)=0$	V = 4000 (V)
Boundaries 3 & 4	$\vec{n}\cdot(-D_e\nabla N_e)=0$	$\vec{n}\cdot(-D_p\nabla N_p)=0$	$\vec{n}\cdot(-D_n\nabla N_n)=0$	$\vec{n}\cdot(\varepsilon_0\varepsilon_r\vec{E})=0$
Boundary 5	$\vec{n}\cdot(\overrightarrow{W_e}N_e - D_e\nabla N_e)=0$	$\vec{n}\cdot(\overrightarrow{W_p}N_p - D_p\nabla N_p)=0$	$\vec{n}\cdot(\overrightarrow{W_n}N_n - D_n\nabla N_n)=0$	$\vec{n}\cdot(\overrightarrow{D_1}-\overrightarrow{D_2})=0$
Boundary 6	-	-	-	$\vec{n}\cdot(\overrightarrow{D_1}-\overrightarrow{D_2})=0$
Boundary 7	-	-	-	V = 0

dielectric interface to simulate the charge accumulation process. The first type sets the fluxes of charged particles to zero; the dielectric acts as an impermeable media. The plasma is hence contained completely in the gas [15, 17]. The second type allows charged particles to go through and the integration of charged particle fluxes yields the surface charge density [3, 11]. The charges accumulate at the surface in this case and are separated from the plasma in the gas. The former approach works best with dynamic structure whereas the latter is suitable for less dynamic cases. For this reason, the former boundary condition was used for the proposed model.

Table 2. *Boundary conditions for the second phase (1D) of the positive surface discharge model*

Charge species	Left boundary	Right boundary
Electrons	$-D_e\frac{\partial N_e}{\partial x}=0$	$W_eN_e - D_e\frac{\partial N_e}{\partial x}=0$
Positive ions	$W_pN_p - D_p\frac{\partial N_p}{\partial x}=0$	$-D_p\frac{\partial N_p}{\partial x}=0$
Negative ions	$-D_n\frac{\partial N_n}{\partial x}=0$	$W_nN_n - D_n\frac{\partial N_n}{\partial x}=0$

The second phase of the model is simplified to 1D as the streamer is assumed to occupy a cylindrical channel of fixed radius. Charge densities vary along the channel axis but remain uniform at each cross-section. The continuity equations 1 - 3 were rewritten in 1D and solved using the accurate finite-volume flux-corrected transport (FV-FCT) algorithm [23]. The Boris-Book limiter has been utilised due to ease of implementation as compared to the equivalently good Zalesak limiter. A time step of 10^{-13} s and a uniform mesh of 1μm size were chosen. These parameters were selected to ensure the Courant-Friedrichs-Lewy (CFL) number much less than 0.5 for stability purposes. Boundary conditions in phase II are summarised in Table 2.

Poisson's equation 4 in phase II was solved by a revised disc method. In this method, the streamer channel is divided into minute discs and the total space charge field is calculated as an integration of the field generated from each disc [19, 24]. The channel radius chosen in this simulation was 50μm as this value has been measured experimentally and commonly used in gas discharge simulations [10, 25, 26]. The influence of this parameter on the discharge development is also studied in this paper. A thickness of 4 μm was chosen for each minute disc as it has been shown to produce good field results with acceptable computational run time [19]. The revised disc method used in this work assumes that image charges on the metal electrode and dielectrics play a minor role in the field calculation. In order to justify this assumption, a comparison between the field calculated using the disc method and that calculated by the finite element analysis in 3D has been made using the same space charge distribution [19]. It has been concluded that the revised disc method is acceptably accurate to be used in surface

discharge modelling. The difference between the field magnitudes obtained from both methods is under 10%.

4. Simulation results

4.1. Phase I

A Gaussian distribution of neutral plasma (seed electrons and positive ions) with the peak value of 10^{14} m^{-3} and width of 25μm was set at the needle tip to commence the discharge [14, 19]. The initial plasma distribution has been confirmed to only speed up the streamer formation process and not affect the streamer characteristics [26]. The source term *S* in equations 1 - 2 indicates the rate of electron-ion pairs generated from the photoionisation process and was simulated as $10^{26}m^{-3}s^{-1}$ in this model [14, 18]. This is a simple approximation to realise processes caused by radiated photons in the gas and has been utilised by some authors [27, 28]. In order to have a similar voltage waveform to that used in the experiment, a step voltage of 4kV was used in the simulation.

Simulation results obtained in the first phase are presented in Fig.s 3 - 7. The first observation is that the streamer travels in the gas gap as an ionising wave. This structure is characterised by a moving streamer head which has a strong electric field and a quasi-neutral density stem behind it. Fig. 3 shows the 2D electric field distribution at various times up until the instant the streamer reaches the dielectric surface. When the streamer has fully developed in the gas (0.4ns) its radial field expansion reaches around 200μm. The streamer head width falls in the range from 50 - 100μm. The axial field plot along the symmetry axis, Fig. 5(d), clearly shows the changes in the magnitude of the streamer head field. The streamer forms after about 0.1ns and the streamer head field decreases while traversing across the gap. After 0.5ns the maximum field strength reduces from 7.2×10^7V/m to 2×10^7V/m. When the streamer reaches the vicinity of the dielectric with high permittivity the streamer head field is enhanced greatly (0.575ns curve). At this interface region, the electric field changes its magnitude and shape.

Fig. 4 shows the 2D positive ion and electron density distributions at various times at which the respective field distributions in Fig. 3 are plotted. As shown in Fig. 5(c) the negative ion density is of one order lower than the others; its contribution to Poisson's equation is negligible

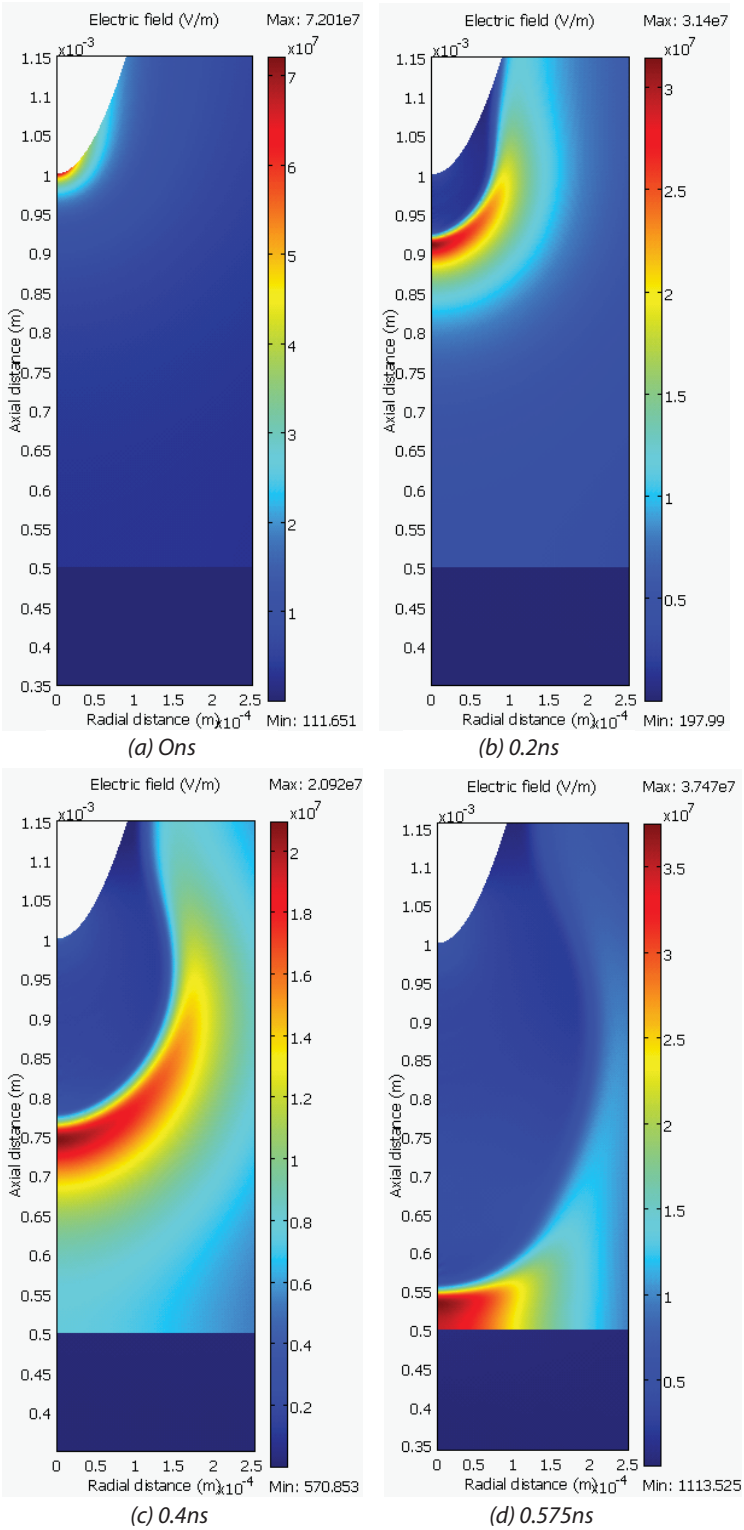

Fig. 3. *2D electric field distribution at various times in phase I*

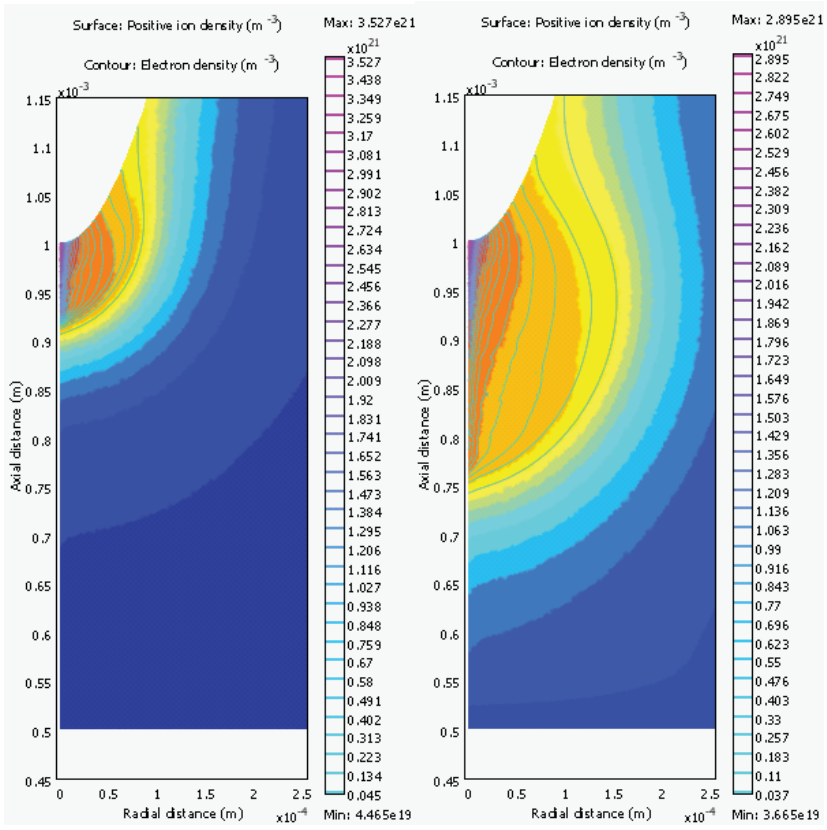

(a) 0.2ns *(b) 0.4ns*

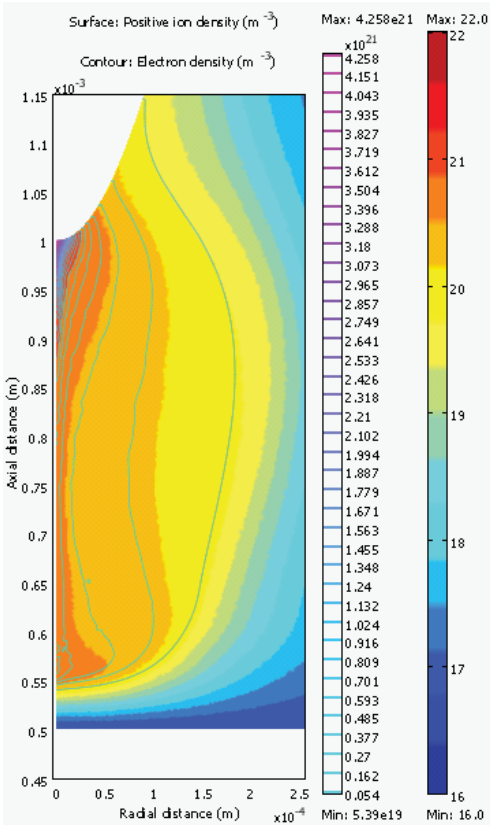

(c) 0.575ns

Fig. 4. *2D positive ion and electron density distributions at various times in phase I*

and is hence not shown in the 2D plots. Both positive ions and electrons are highly concentrated in a narrow volume along the symmetry axis (approximately $2 \times 10^{21} m^{-3}$) then quickly drop radially. The radial expansion of these species can be approximated to about 200 μm from the 2D plots. The electron density distribution follows that of positive ions to a good extent. The electron density is slightly lower than the positive ion density and displaced by a tiny distance towards the needle electrode, Fig. 5. This can be attributed for by the difference in mobility of electrons and positive ions and the fact that electrons are constantly sucked into the stem of the streamer and ultimately the anode. The positive ions, on the other hand, remain almost stationary where they are created. Electron attachment process also plays a role causing to the difference in the charge density magnitude. The displacement creates a positive net charge at the head and a quasi-neutral plasma in the stem. This explains the formation of the streamer head field. As the streamer advances and before reaching the dielectric, both charge densities drop to approximately $3.5 \times 10^{20} m^{-3}$. The densities start increasing as the streamer interacts with the dielectric surface.

In order to calculate the velocity of the streamer in phase I, the peak of the electric field is recorded as a function of time and distance. Fig. 6 shows the streamer velocity during its propagation in the gas gap. It is clear that the velocity increases as the streamer advances. The peak velocity obtained is just under $1.5 \times 10^{6} m/s$ at the position where the streamer is about to interact with the dielectric surface. After the peak, the streamer slows down to commence its radial development.

In order to determine the instant just before the streamer starts spreading

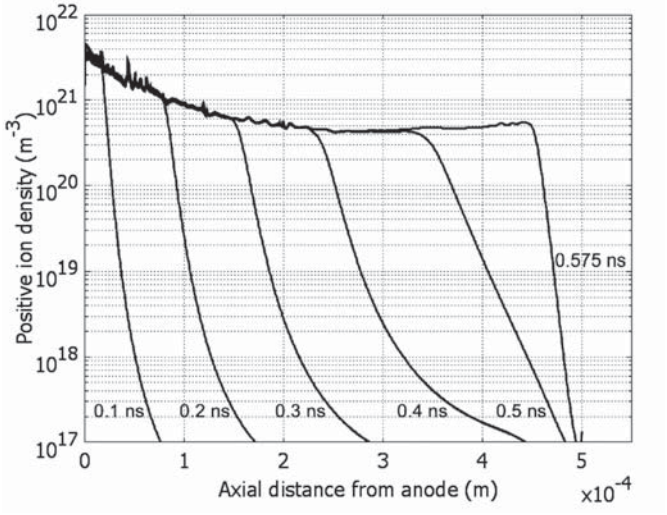

(a) Positive ion density distributions along the symmetry axis

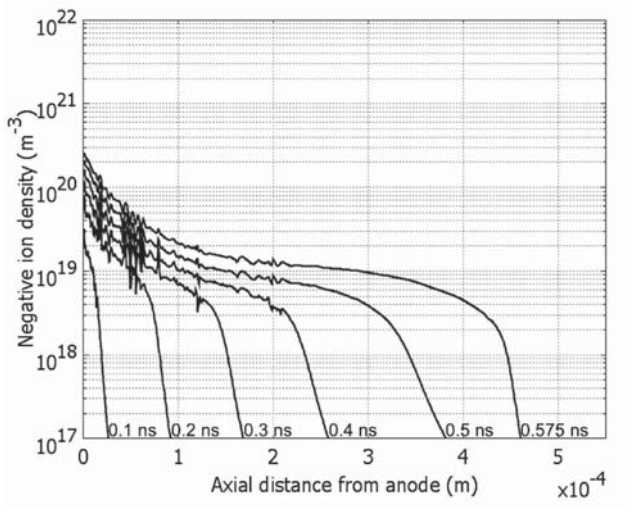

(c) Negative ion density distributions along the symmetry axis

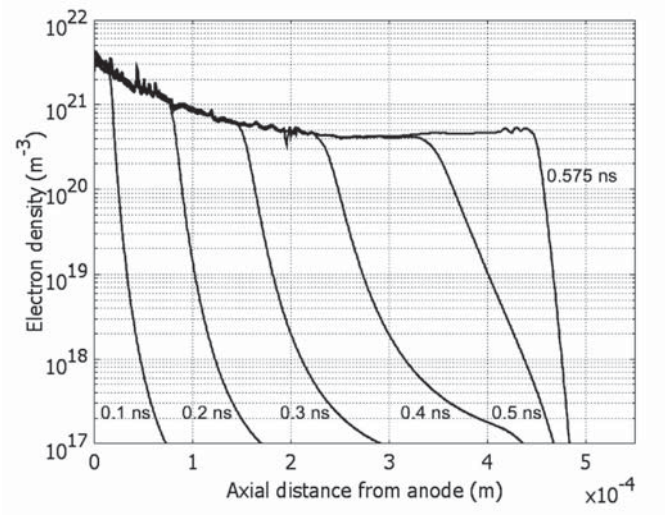

(b) Electron density distributions along the symmetry axis

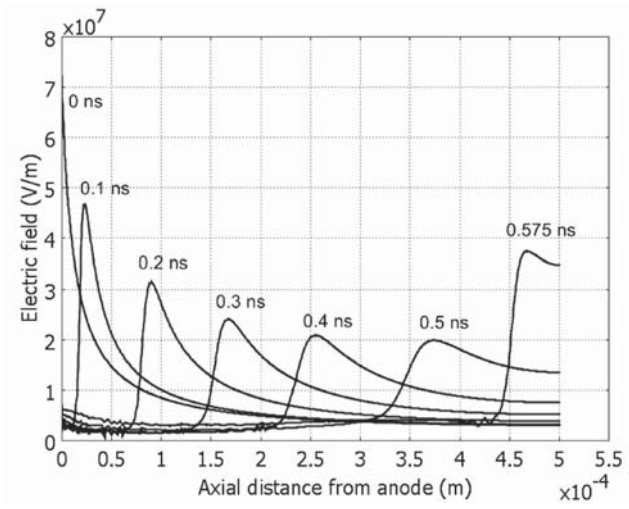

(d) Electric field distributions along the symmetry axis

Fig. 5. *Charged particle density and electric field distributions along the symmetry axis at various times in phase I*

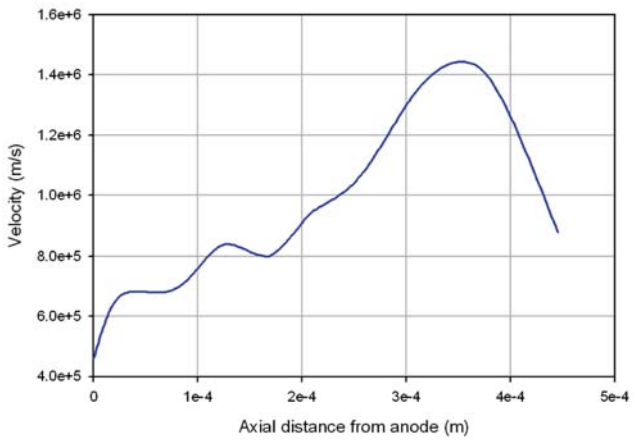

Fig. 6. *Streamer velocity versus distance in phase I*

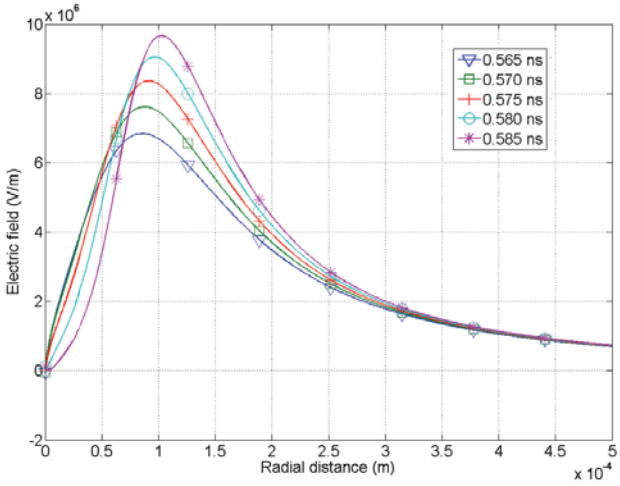

Fig. 7. *Radial electric field distribution at various times in phase I at 50μm above the dielectric surface*

out over the dielectric in the 2D axial symmetry space dimension, the plot of the radial field against distance at 50μm above the dielectric surface at various times was investigated. This plot is shown in Fig. 7. As can be observed, the radial field increases at a fast rate when the streamer approaches the dielectric. After 0.575ns, the streamer starts to move radially indicated by the movement of the electric field peak and the drop in the field near the symmetry axis. The radial field at 0.575ns was hence used as the driving force for the second phase of the simulation. The field peak reaches 8.2×10^6V/m at this time instant.

4.2. Phase II

Phase II of the simulation starts by using the radial field obtained at 0.575ns from the first phase as the initial electric field. It should be noted that measured streamers branch out from the centre of the insulator hence this phase only simulates the development of one streamer. It was assumed that the cylindrical streamer channel propagates directly above the BSO surface. All other parameters were kept the same as specified in phase I including the initial density conditions. The simulation results of the streamer propagating along the dielectric surface are shown in Fig.s 8 - 11. The first observation is that the streamer has the same ionising wave structure as in phase I. The streamer comes to a stop at around 3mm after 106ns with the specified parameters. At this point, the streamer head field is lower than the ionisation level in air (approximately 3×10^6V/m). As the streamer head field collapses, the field near the symmetry axis tends to increase back to the initial field due to the reduced effect of the space charge. The velocity plot (Fig. 9) clearly shows that the streamer in this phase undergoes two different stages during its propagation: the acceleration and deceleration. Near the origin, the streamer accelerates away until the maximum velocity of 8×10^4m/s is reached at around 0.6mm. It is then followed by the deceleration regime when streamer reaches the decaying tail of the initial field. The velocity in phase II is about 15 times less than that found in phase I. This can be accounted for by the fact that in phase I the initial applied field is much stronger (approximately 10 times) over a much shorter gap and also because of the field enhancement effect when the streamer interacts with the dielectric in phase I. The maximum velocity calculated in phase II is in good agreement with the experimentally measured values reported in [10, 29]. The electron and positive ion density profiles at three selected instants in time are shown in Fig. 10. It is evident that using the FCT algorithm the charge profiles are much smoother than those obtained from the finite element method in phase I. The positive ion density ($3 - 8 \times 10^{19}$m^{-3}) is clearly higher than the electron density everywhere due to the high mobility of electrons and their movement towards the left boundary. Both the electron and positive ion densities drop as the streamer advances. The negative ion density in this phase is of the order of 10^{17} m^{-3} and does not play a role in the streamer propagation as in the previous phase. The charge density in this phase is lower than that obtained in the previous phase due to the difference in the magnitude of the initial field.

The net charge density distribution presented in Fig. 11 evidently shows its correlation with the streamer head field. The net charge distribution is characterised with a high gradient spike at the front and a quasi-constant lower-density charge distribution in the stem. Near the origin, there is a negative charge region due to the high concentration of negative ions at low electric field. At 4 ns, the net charge spike has a sharp gradient and high magnitude (6×10^{19}m^{-3}). As the streamer develops, the spike becomes shorter and less sharp. After 90ns, the streamer

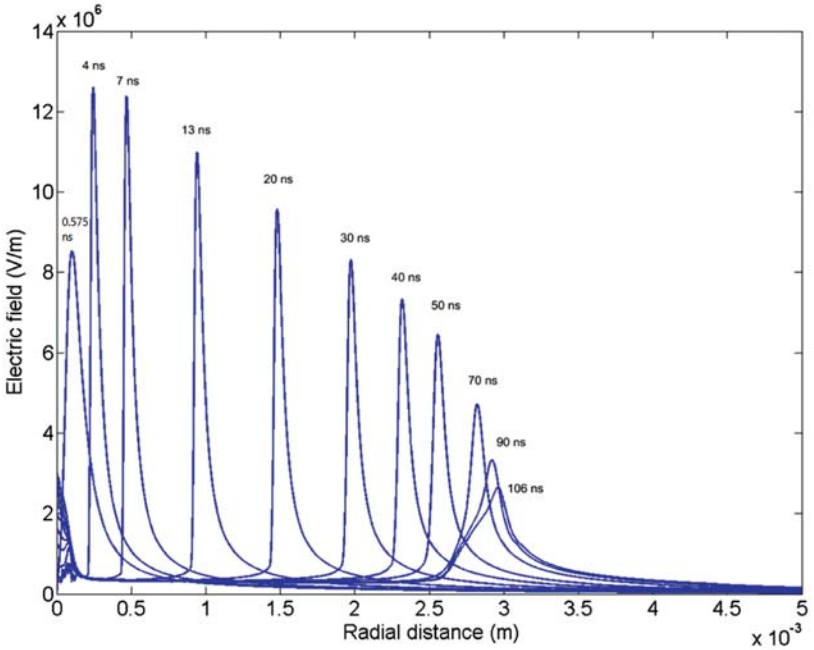

Fig. 8. *Electric field distribution at various times in phase II*

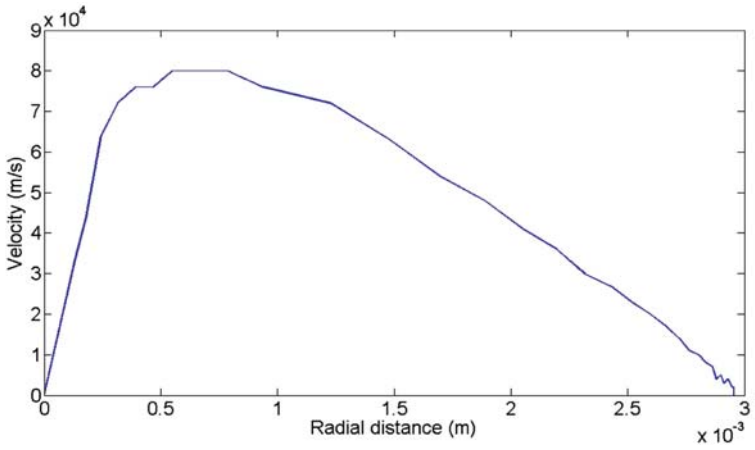

Fig. 9. *Streamer velocity versus distance in phase II*

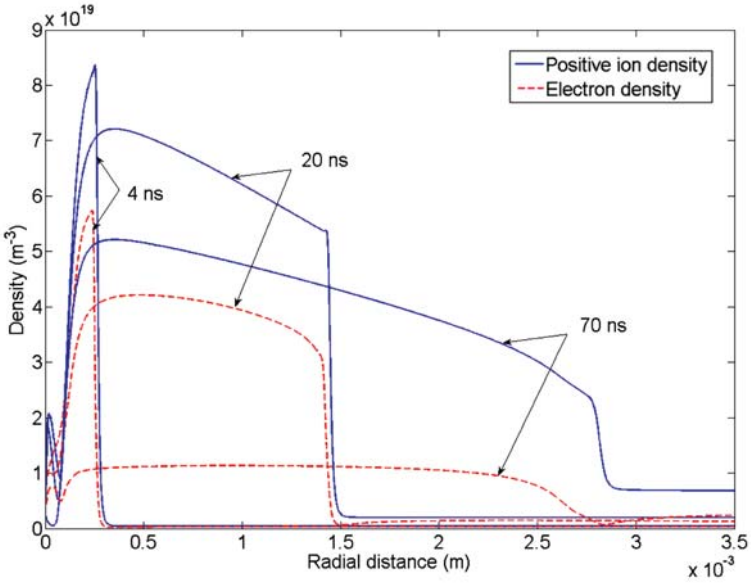

Fig. 10. *Electron and positive ion density distributions at 4, 20 and 70ns in phase II*

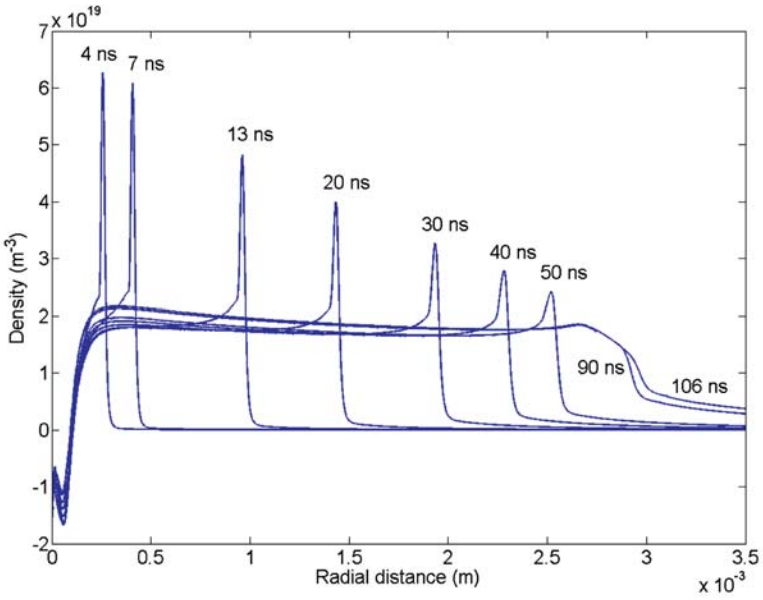

Fig. 11. *Net charge density distributions in phase II*

has travelled around 3mm and the net charge spike has a value lower than the maximum density in the stem of the streamer channel. The streamer totally collapses after 106ns; at this instant the net charge spike flattens and the streamer head field drops below 3×10^6V/m. The streamer length in this case is calculated as 3 mm which is in reasonable agreement with experimental results [10].

5. Comparison with experimental measurements

The Pockels method has been used to measure surface discharge under 4kV magnitude and 5ms square voltage waveform at atmospheric pressure. The 2D surface charge density distribution is shown in Fig. 12(a) while the line charge density along the dashed line (XY) is shown in Fig. 12(b). The discharge produces streamers of 4.5mm long and 0.7nCmm^{-2} density in average. The model proposed earlier predicts a streamer length of about 3mm. Nonetheless, the effects of the background ionisation and streamer radius have been investigated and it is confirmed that the streamer length is inversely dependent on the variation of these parameters. Hence in order to match the experimental streamer length a smaller background ionisation value or a smaller streamer radius can be used. As the streamer radius of 50μm has been widely used in the literature, this section presents a result comparison for the case of the background ionisation reduced to 5×10^{25}m^{-3}s^{-1}.

Fig. 13 demonstrates the evolution of the net charge density in the second phase of the model using this background ionisation value. It is clear that the streamer collapses at the distance of about 4.3 mm which is closer to the experimental measurement. Since the simulation provides the plasma space charge density, it is not possible to directly compare this quantity with the surface charge density measured from the Pockels experiment. However, comparison can be made between the electric field induced across the BSO crystal (*z*-component) due to the experimental surface charge and that due to the simulation space

charge. According to the electro-optic theory, this is the quantity the Pockels technique measures. The relationship between this electric field component and surface charge density takes the form

$$E_{z(x,y)} = \frac{\sigma_{(x,y)}}{2\varepsilon_0\varepsilon_r} \quad (5)$$

In order to calculate the *z*-component electric field due to the net space charge density, numerical modelling was required. The finite element method has been utilised in 3D for this analysis. The discharge geometry detailed in Fig. 2 was extended to 3D with a streamer set on top of the BSO layer - Fig. 14(a). The streamer is made of a 50μm radius and 4.3mm long cylinder. The charge density within this cylinder was set constant at $2 \times 10^{19} m^{-3}$ because this is the charge density in the stem of the streamer channel during both the acceleration and deceleration stages. The effect of the high density spike traversing across the dielectric surface is negligible since the streamer development duration (150ns) is much shorter than the camera exposure time (100 - 200μs). The recorded data is integrated images showing the field induced by the space charge density in the streamer stem. The *z*-component electric field was solved and the cross-sectioned distribution on the plane perpendicular to the BSO surface and going through the centre of the streamer is shown in Fig. 14(b). The impact of the space charge on the electric field across the BSO crystal is evident in this figure. Inspection of the *z*-component field along the *z* axis across the 160μm thick BSO shows that the field varies linearly. Hence the average electric field in the BSO can be found at a distance of 80μm below the top surface (dashed line in Fig. 14(b)). The plot of the electric field distributions obtained along this line and from the experimental surface charge is shown in Fig. 14(c). It can be seen that the simulation field is about one fifth of the experimental measurement. This fact suggests that charge injection into the insulator bulk is one of other factors contributing to the measured field.

6. Conclusion

The positive surface discharge has been simulated in two phases using the hydrodynamic drift-diffusion approximation. The first phase which involves the axial development of streamer in the gas gap was solved in 2D axial symmetry space dimension

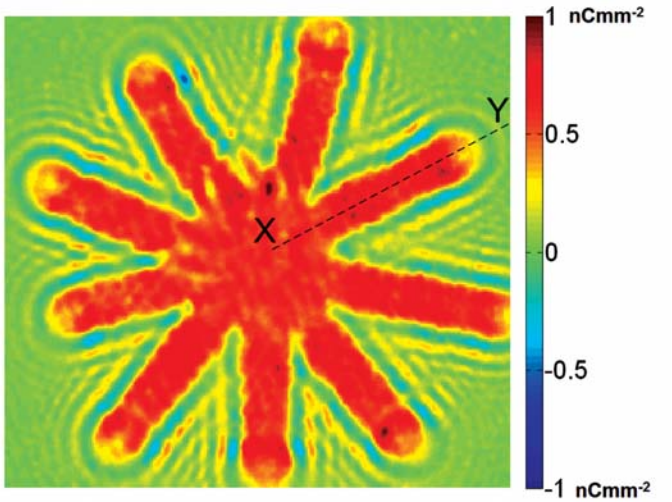

(a) 2D surface charge density distribution

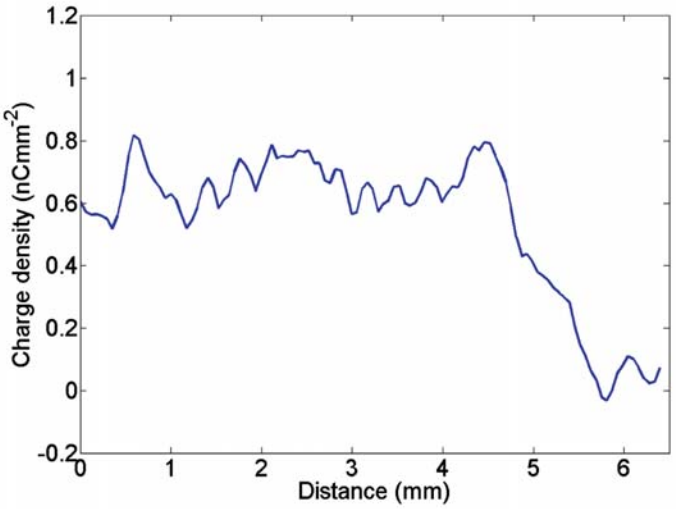

(b) Line charge density distribution

Fig. 12. *Experimental Pockels results obtained under 4kV magnitude 5ms duration positive square voltage waveform*

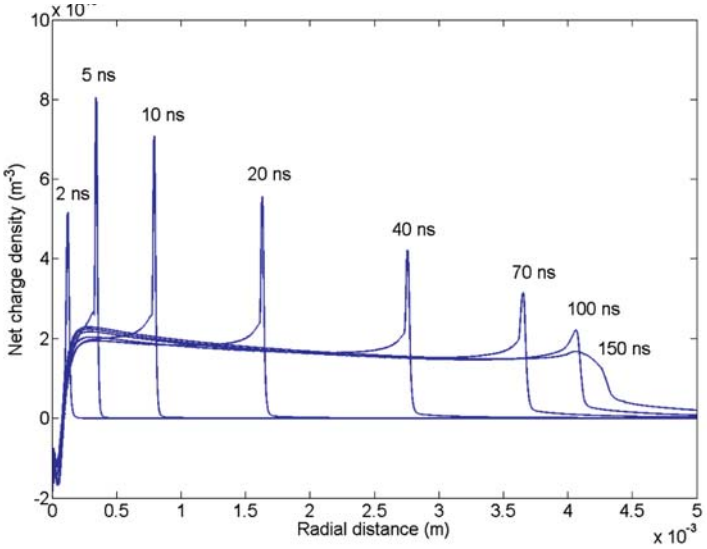

Fig. 13*. Phase II net charge density evolution for the positive surface discharge simulation obtained from* $S = 5 \times 10^{25} m^{-3} s^{-1}$

using the finite element analysis. The second phase uses the field results from the first phase and simulates the radial streamer propagation along the dielectric surface. This phase was simulated in 1D using the accurate FCT algorithm adopting some reasonable simplifications. The following observations have been made:

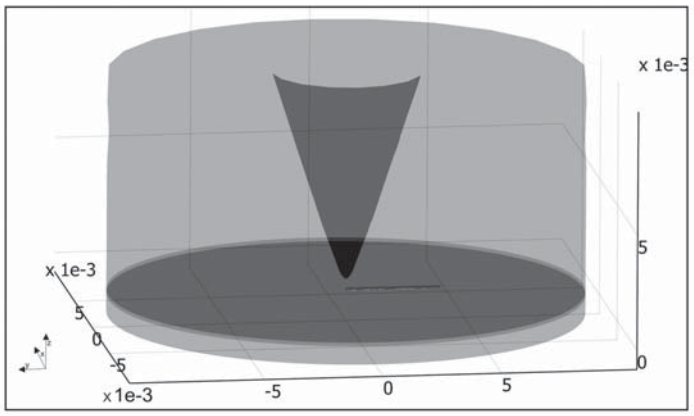

(a) 3D charge density distribution

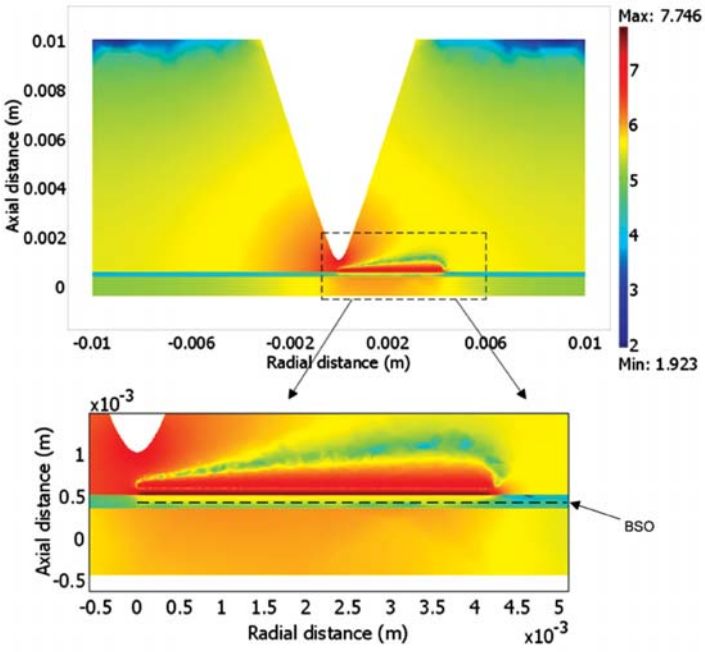

(b) Cross-sectioned z-component electric field distribution in log scale

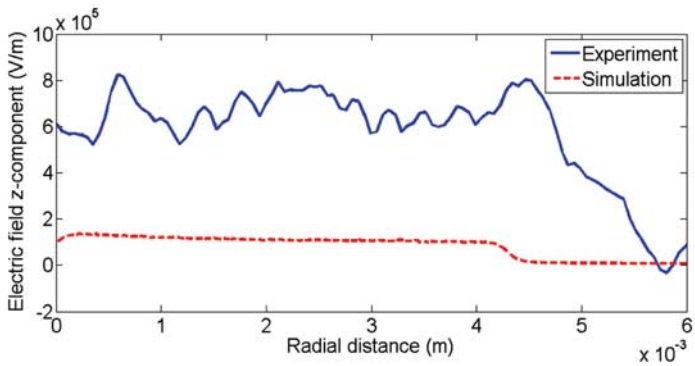

(c) z-component electric field distribution comparison

Fig. 14. *Comparison between simulation and experimental positive surface discharge results*

- The streamer shows the ionising wave structure in both phases. The streamer dynamics are strongly dependent on the electric field created by the dielectric barrier. In phase I, the streamer accelerates when it is about to interact with the dielectric surface.

- Phase II shows the acceleration stage followed by the deceleration. The field magnitude, charge densities and velocity are all smaller than in phase I.

- The simulation and experimental results have a good agreement in terms of streamer length when the ionisation source term of $5 \times 10^{25} m^{-3}$ is used. The *z*-component electric field obtained from the simulation is one fifth of the experimental measurement at atmospheric pressure.

References

1. Georghiou G E, Papadakis A P, Morrow R and Metaxas A C. *Numerical modelling at atmospheric pressure leading to plasma production* J. Phys. D: Appl. Phys. 2005; 38: p. 303 - 328.

2. Kogelschatz U. *Dielectric-barrier discharges: their history, discharge physics, and industrial applications*. Plasma Chemistry and Plasma Processing. 2002; 23: p. 1 - 46.

3. Lagmich Y, Callegari T, Pitchford L and Boeuf J. *Model description of surface dielectric barrier discharges for flow control*. J. Phys. D: Appl. Phys. 2008; 41.

4. Manabe Y and Shimazaki T. *Formation mechanism of surface corona on dielectric plates under negative impulse voltage in atmospheirc air*. IEEE Transactions on Dielectrics and Electrical Insulation. 2004; 11(4): p. 631 - 637.

5. Celestin S, Allegraud K, Canes-Boussard G, Leick N, Guaitella O and Rousseau A. *Patterns of plasma filaments propagating on a dielectric surface*. IEEE Transactions on Plasma Science. 2008; 36 (4): p. 1326 - 1327.

6. Tanaka D, Matsuoka S, Kumada A and Hidaka K. *Two-dimensional potential and charge distributions of positive surface streamer* J. Phys. D: Appl. Phys. 2009; 42 075204.

7. Timatkov V V, Pietsch G J, Saveliev A B, Sokolova M V and Temikov A G. *Influence of solid dielectric on the impulse discharge behaviour in a needle-to-plane air gap*. J. Phys. D: Appl. Phys. 2005; 38: p. 877.

8. Akyuz M, Cortet P P and Cooray V. *Positive streamer discharges along liquid dielectric surfaces: effect of dielectric constant and surface properties*. IEEE Transactions on Dielectrics and Electrical Insulation. 2005; 12 (3): p. 579 - 585.

9. Sam Y L, Lewin P L, Davies A E, Wilkinson J S, Sutton S J and Swingler S G. *Surface discharge measurements of polymeric materials*. IEE Proceedings: Science, Measurement and Technology. 2003; 150: p. 43 - 52.

10. Murooka Y, Takada T and Hidaka K. *Nanosecond surface discharge and charge density evaluation, part i: review and experiments*. IEEE Electrical Insulation Magazine. 2001; 17 (2): p. 6 16.

11. Tran T N, Golosnoy I O, Lewin P L and Georghiou G E. *Numerical modelling of negative discharges in air with experimental validation*. J. Phys. D: Appl. Phys. 2011; 44 015203.

12. I Gallimberti. *A computer model for streamer propagation* .J. Phys. D: Appl. Phys. 1972; 5: p. 2179 - 2189.

13. Morrow R and Lowke J. *Streamer propagation in air*. J. Phys. D: Appl. Phys. 1996; 30: p. 614 - 627.

14. Ducasse O, Papageorghiou L, Eichwald O, Spyrou N and Yousfi M. *Critical analysis on two-dimensional point-to-plane streamer simulations using the finite element and finite volume methods.* IEEE Transactions on Plasma Science. 2007; 35 (5): p. 1287 - 1298.

15. Papageorghiou L, Panousis E, Loiseau J, Spyrou N and Held B. *Two-dimensional modelling of a nitrogen dielectric barrier discharge (DBD) at atmospheric pressure: filament dynamics with the dielectric barrier on the cathode*. J. Phys. D: Appl. Phys. 2009; 42 (8): p. 105201 - 105210.

16. Kumara S, Serdyuk Y and Gubanski S. *Charging of polymeric surfaces by positive impulse corona*. IEEE Transactions on Dielectrics and Electrical Insulation. 2009; 16 (3): p. 726 - 733.

17. Celestin S, Bonaventura Z, Guaitella O, Rousseau A and Bourdon A. *Influence of surface charges on the structure of a dielectric barrier discharge in air at atmospheric pressure: experiment and modeling European Physical*. Journal Applied Physics. 2009; 47 (2): p. 22810 - 22815.

18. Hallac A, Georghiou G and Metaxas A. *Secondary emission effects on streamer branching in transient non-uniform short-gap discharges* J. Phys. D: Appl. Phys. 2003; 36: p. 2498 - 2509.

19. Tran T N. *Surface discharge dynamics: theory, experiment and simulation*. PhD Thesis, University of Southampton, UK. 2010.

20. O'Sullivan F M. *A model for the initiation and propagation of electrical streamers in transformer oil and transformer oil based nanofluids.* PhD Thesis, MIT. 2007.

21. Lee S H, Lee S Y, Chung Y K and Park I H. *Finite-element analysis of corona discharge onset in air with artificial diffusion scheme and under Fowler-Nordheim electron emission.* IEEE Transactions on Magnetics. 2007; 43: p. 1453 - 1456.

22. Georghiou G E, Morrow R and Metaxas A C. *An improved finite-element flux-corrected transport algorithm*. Journal of Computational Physics. 1999; 148: p. 605 - 620.

23. Boris J and Book D. *Flux-corrected transport. iii. minimal-error FCT algorithms.* Journal of Computational Physics. 1976; 20: p. 397 - 431.

24. Davies A, Evans C and Jones F. *Electrical breakdown of gases: the spatiotemporal growth of ionisation.* In fields distorted by space charge Proceedings of the Royal Society of London. 1964; 281 (A): p. 164 - 83.

25. Tanaka M, Murooka Y and Hikada K. *Nanosecond surface discharge development using the computer simulation method*. J. Appl. Phys. 1987; 61 (9): p. 4471 - 4478.

26. Georghiou G. *Gas discharge modelling using the finite-element flux-corrected transport method.* PhD Thesis. University of Cambridge, UK. 2000.

27. Dhali S and Williams P. *Two-dimensional studies of streamers in gases.* J. Appl. Phys. 1987; 62 (12): p. 4696 - 4707.

28. Vitello P, Penetrante B and Bardsley J. *Simulation of negative streamer dynamics in nitrogen*. Phys. Rev. E. 1994; 49 (6): p. 5574 - 5598.

29. Allen N and Mikropoulos P. *Streamer propagation along insulating surfaces.* IEEE Transactions on Dielectrics and Electrical Insulation. 1999; 6 (3): p. 357 - 362.